IEEE Access
Multidisciplinary | Rapid Review | Open Access Journal

Received 10 September 2024, accepted 24 September 2024, date of publication 2 October 2024, date of current version 10 October 2024.

Digital Object Identifier 10.1109/ACCESS.2024.3470652

RESEARCH ARTICLE

An Optimal Energy Dispatch Management System for Hybrid Power Plants: PV-Grid-Battery-Diesel Generator-Pumped Hydro Storage

FATMA AHMED[1], (Graduate Student Member, IEEE), RASHID AL-ABRI[2], (Senior Member, IEEE), HASSAN YOUSEF[2], AND AHMED M. MASSOUD[1], (Senior Member, IEEE)

[1]Department of Electrical Engineering, Qatar University, Doha, Qatar
[2]Department of Electrical and Computer Engineering, Sultan Qaboos University, Muscat 123, Oman

Corresponding author: Fatma Ahmed (fa1702175@qu.edu.qa)

This work was supported by the International Research Collaboration Co-Fund (IRCC), Qatar University, under Grant IRCC-2022-609.

ABSTRACT Effective real-time energy management strategies are crucial for optimising hybrid power plants, particularly when challenged with integrating Renewable Energy Sources (RESs) and managing their intermittent nature. This paper presents a comprehensive energy management framework holding real-time optimisation for HPP. The practical implications of this research are significant, as it provides a roadmap for seamlessly integrating RESs with Battery Energy Storage Systems (BESSs) in Hybrid Power Plants (HPPs) to minimise cost while meeting daily household energy demands. Furthermore, it demonstrates how diesel generators (DGs) can be incorporated into the HPP's energy management system while minimising carbon emissions. An Energy Dispatch Engine (EDE) is introduced to control HPPs that combine PV, BESS, DG and Pumped Hydro Storage (PHS). Two optimisation approaches are used, namely, Mixed-Integer Linear Programming (MILP) and Stochastic Dual Dynamic Programming (SDDP). The system leverages load and RES power data while considering State-of-Charge (SoC) constraints to manage battery health proactively. Optimising discharge and charge profiles of the BESS, with the overarching goal of minimising the total cost of satisfying daily load demand, is an objective. Various tariff schemes were explored to assess the presented EDE. Our testing demonstrates that the SDDP approach consistently results in lower total costs than MILP. The total cost for the MILP method, where the system with PHS incurs higher costs (219.8 $/24h) than the total cost for the SDDP method, where the system with PHS system (180 $/24h). The cost of CO2 emissions was found to be lower in the case of SDDP, amounting to 8.3 $/24h for a total emission of 160 kg. In contrast, the MILP approach resulted in a higher CO2 cost of 10.2 $/24h for a total emission of 200 kg. This suggests that SDDP is more cost-effective in terms of reducing CO2 emissions.

INDEX TERMS Energy dispatch engine (EDE), mixed integer linear programming (MILP), stochastic dual dynamic programming (SDDP), energy management system (EMS), hybrid power plant (HPP), optimization.

NOMENCLATURE

Indices

$t(T)$	Index (set) of time periods.
$n(N)$	Index (set) of the length of the forecasted rolling horizon.

Variables

P_{ess}	Battery Energy Storage Power (kW).
P_l	Load Power (kW).
Q-ESS	Maximum Capacity of the ESS.
η_{ESS}	Charger efficiency (%).
Δt	Time interval (min).
η_p	Pump efficiency (%).
η_b	Battery Efficiency (%).

The associate editor coordinating the review of this manuscript and approving it for publication was Cuo Zhang.

η_t	Turbine efficiency (%).
$\forall_{intial}$	The initial volume of the water in the reservoir.
E_R	Nominal potential energy of the reservoir in (kWh).
α_{co_2}	Gas mass (kg/L).
C_f	Cost of fuel ($/L).
P_{pv}	Power of the photovoltaic (MW).
P_{DG}	Power of the diesel generator (MW).
k	Power Temperature Coefficient ($\%/°C$).
T_{pv}	PV's cell Temperature ($°C$).
G	Solar Radiation $\left(\frac{W}{m^2}\right)$.

Abbreviation

CPP	Critical Peak Pricing.
DG	Diesel Generator.
EDE	Energy Dispatch Engine.
EMS	Energy Management System.
HPPES	Hybrid Power PlantEnergy System.
MILP	Mixed Integer Linear Programming.
PV	Photovoltaic.
PHS	Pumped Hydro Storage.
RES	Renewable Energy System.
RTP	Real-Time Pricing.
SDDP	Stochastic Dual Dynamic Programming.
SoC	State of Charge.
TOU	Time-of-Use.

I. INTRODUCTION

The rapid adoption of Renewable Energy Sources (RESs) in power systems over the past two decades has introduced significant challenges, particularly in balancing energy supply and demand due to the intermittent nature of sources like photovoltaic (PV) systems. One of the primary challenges is the effective integration of RESs with existing grid infrastructure, which may result in a fluctuating power supply, causing grid instability. Grid-connected energy storage systems (ESSs) can help improve the grid's reliability and security. However, they might not always provide an effective techno-economic solution in large-scale power systems applications. Developing a proper energy management system (EMS) supports optimal energy dispatch, particularly with hybrid power plants, alleviating the challenges encountered. To address these issues, this study focuses on developing a comprehensive energy dispatch management system for hybrid power plants (HPPs) that combine PV, Battery Energy Storage Systems (BESS), Diesel Generators (DG), and Pumped Hydro Storage (PHS). By optimising the energy dispatch using advanced algorithms, we aim to enhance the reliability and efficiency of the power supply within a microgrid, reduce operational costs, and minimise carbon emissions. The proposed Energy Dispatch Engine (EDE) leverages Mixed-Integer Linear Programming (MILP) and Stochastic Dual Dynamic Programming (SDDP) to optimise the operation of HPPs. This dual optimisation approach allows for more robust decision-making under uncertainty, significantly reducing operational costs and carbon emissions compared to Conventional methods. The flexibility of our system to scale from small microgrid applications to larger power systems demonstrates its potential for widespread impact in the energy sector, supporting the scalability and broader applicability in a similar fashion to [1] and [2]. It is essential to raise the effectiveness and efficacy of these hybrid PV-Grid-ESS power plants [3]. With a simple and effective technique for optimisation, the optimal grid interconnection of PV and ESS, along with the energy dispatch strategy, can be optimally identified. This can lower energy expenses, increase system effectiveness, and reduce the HPP's environmental impact [4]. EMS optimisation techniques can be categorised into three types based on complexity: intelligent, metaheuristic, and classical approaches. Innovative techniques employ neural networks that incorporate weighted variables to optimise power transfer, but they are computationally demanding [5]. Metaheuristic methods, such as Monte Carlo simulations, random simulation, and search algorithms, such as Genetic Algorithm, Grey-Wolf, and Particle Swarm Optimization (PSO), are employed to optimise an objective function without or without constraints [6]. Although less computationally intensive than intelligent methods, metaheuristic methods typically require more time to solve optimisation problems. Conventional approaches are based on mathematical principles and strive to optimise an objective function while adhering to a specified set of constraints. These methods often rely on predetermined initial values and predefined parameters, as seen in Linear and Non-Linear Programming (LP/NLP) and Mixed-Integer Linear and Non-Linear Programming (MILP/MINLP) [15]. ESS was used to manage unpredictable wind power fluctuations, aided by accurate predictions through Artificial Neural Networks (ANN). This hybrid ESS supports optimising schedules based on forecasts and real-time adjustments, leading to economic benefits for RESs by aligning energy output with pricing signals [7]. In [8], a strategy has been outlined for dispatching a wind-solar hybrid power system using a hybrid ESS comprising batteries and supercapacitors. The approach optimises battery and supercapacitor use for cost-effective energy storage. The hybrid ESS cost optimisation is achieved through the filter's time constant using curve fitting and PSO. Simulation results validate the approach's superiority over the single storage method, achieving accurate power dispatch and advancing RES integration with optimised ESSs. The authors in [9] Presented the power flow challenges in distribution networks due to increased RESs and flexible loads. It introduces Virtual Power Plants (VPPs) to integrate various energy sources and improve RES utilisation. A two-stage congestion management model involving Independent System Operator (ISO) congestion management and VPPs with hybrid generators was presented. The first stage minimizes congestion costs through a genetic algorithm, while the second stage considers multi-objective

TABLE 1. Literature review comparison.

Reference	Hybrid system configuration					Optimisation method	Real-Time
	RES	CO2	Fuel/ DG	ESS	Water		
[7]	✓	×	×	✓	✓	ANN	✓
[8]	✓	×	×	✓	×	Particle Swarm Opt. (PSO)	✓
[9]	✓	×	×	✓	×	Genetic Algorithm (GA)	×
[10]	✓	×	×	✓	×	MPC	✓
[11]	✓	×	✓	✓	×	GA	✓
[12]	✓	✓	✓	✓	×	Stochastic	✓
[13]	✓	×	×	✓	×	Multi-stage stochastic, SDDP	✓
[14]	✓	×	✓	✓	×	NSGA+PSO	×
Proposed	✓	✓	✓	✓	✓	MILP & multi-stage stochastic, SDDP	✓

power correction for VPPs, including water and light curtailment, navigation, and ecological needs. In [10], a dispatch strategy that uses model predictive control (MPC) has been introduced for a wind farm with a dual-battery energy storage system (DBESS). The MPC technique manages the two batteries to alternate between charging and discharging, aligning with the dispatch sequence. Simulation results based on real wind power data confirm the effectiveness of this MPC-based approach. It improves wind farm dispatch coordination with the hybrid wind/battery storage system, enhancing control and introducing a longer lifespan for the battery. The strategy performs well across various scenarios, adeptly following dispatch curves and maintaining the battery state of charge (SoC) within limits. However, the authors in [11] delved into a comprehensive evaluation of a hybrid PV/Deisel Generator (DG)/BESS system's practicality, economic aspects, and energy management. The system targets a specific load far from the utility grid. Key considerations include addressing water demands, reverse osmosis unit sizes, energy dispatch strategies, and DG capacities. The optimal system size is determined based on criteria such as energy cost and environmental impact. An approach has been presented in [12]. The approach combined hybrid stochastic-robust optimization with power flow calculation aiming to reduce CO2 emissions by integrating RESs. The method optimizes power system operation to minimize CO2 emissions via improved generator, load, and energy storage operation, and by evaluating system changes. In [13], an advanced real-time energy management strategy for residential PV-storage hybrid systems comprising solar PV generation and BESS has been presented. It overcomes the challenges of offline and online methods by integrating an offline optimization model with a real-time rule-based controller. Through rolling horizon optimization and deep learning forecasts, the approach effectively reduces electricity purchase costs. It employs a multi-stage stochastic program and the Stochastic Dual Dynamic Programming (SDDP) algorithm for continuous updates to BESS dispatch settings. The approach effectively reduced net electricity purchase costs, validated through simulation tests. The study in [16] focused on optimizing microgrid operations for it enhanced clean energy utilization and cost reduction. It begins by creating a wind power prediction error model incorporating pricing and operational factors of various clean energy sources. Subsequently, a collaborative optimization model for a cooling, heating, and power microgrid is developed, aiming to minimize costs and power-generation units. An intelligent optimization algorithm combining the non-dominated sorting genetic algorithm (NSGA) and beetle antennae search was employed, outperforming the conventional NSGA in simulations on a real microgrid case [16].

TABLE 1 provides a summary of the literature review on RESs in HPPs, comparing the optimization methods and control strategies employed in this paper with those in previous studies. Notably, the proposed concept addresses the HPP comprehensively. In this paper, we introduce an Energy Dispatch Engine (EDE) that leverages MILP and SDDP optimization methods to control a hybrid system consisting of PV, the grid, an ESS, a DG, and Pumped Hydro Storage (PHS) components. This has been done by optimization and comparison of PV/diesel/battery/PHS systems within a multi-objective framework, taking into account factors such as the cost of electricity and CO2 emissions. The paper utilizes load and RES power data while incorporating SoC constraints to manage the battery efficiently. To achieve this, a hybrid system is designed, incorporating PV and a diesel generator

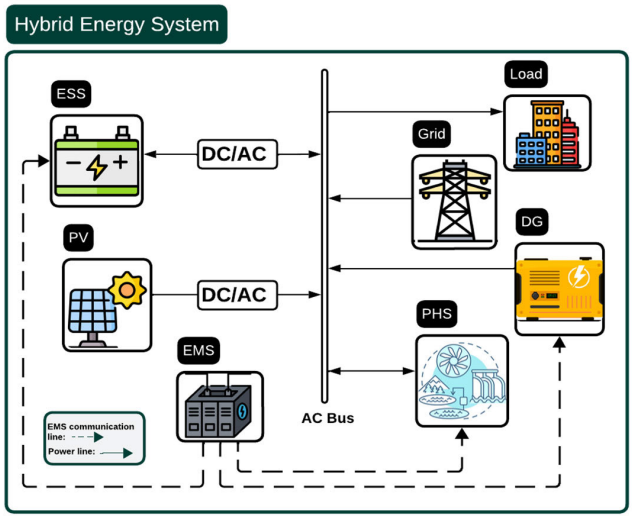

FIGURE 1. Block diagram of the hybrid power plant.

within a multi-objective framework and introducing two types of ESSs, namely, BESS and PHS. The hybrid system is connected to the distribution system, forming a microgrid, which allows for better integration and management of the local energy resources. The effectiveness of the proposed model is evaluated in terms of cost savings by considering three pricing schemes.

The paper is organized as follows: Section II elucidates the methodology and modeling of the proposed real-time optimization. Section III examines the performance of the MILP and SDDP algorithms, along with simulation outcomes. Finally, Section IV provides the paper's conclusion.

II. OPTIMIZATION OF THE HYBRID POWER PLANT

A. DESIGN METHODOLOGY

The schematic of the hybrid HPP in **FIGURE 1** shows that the ESS and PV are connected to the AC grid through an inverter.

1) PV MODELING

To acquire the field data for optimizing the operation of the system, the load and PV power profiles were gathered from Pecan Street data, used in [13], consisting of 1 minute PV power data and load data for 75 homes across the United States in 2018. The instantaneous potential of PV generation is intricately tied to prevailing meteorological conditions, specifically solar irradiance, and ambient temperature, as elucidated in reference [17]. This work assumes that these parameters can be forecasted with acceptable accuracy, which is a plausible assumption. Consequently, at each discrete time increment (t), the electrical output of a PV module (P_{pv}) channeled through an inverter is subject to the dynamic interplay between incident solar radiation (G) and the temperature of the PV cells (T_{pv}), as expounded below [18]:

$$P_{pv} = \eta_{inv}.G\,(t)\,.\left[1 + k\,\left(T_{pv} - 25\right)\right].N_{pv} \qquad (1)$$

where η_{inv} is inverter efficiency, k is the power temperature coefficient ($\%/^{\circ}C$), and N_{pv} is the number of PV modules.

PV power is not treated as a constraint but is dynamically managed to ensure efficient operation. When excess power is generated by the PV system, and the ESS is fully charged, the system implements PV power curtailment to prevent overgeneration. This curtailment is achieved by adjusting the operating point of the PV system or by reducing the power fed into the grid. The EMS continuously monitors the SoC of the ESS, power demand, and grid conditions, and it sends control signals to curtail PV power as necessary to maintain system stability and efficiency [19]. Therefore, the following equation represents the dynamic management of PV power:

$$P_{pv,curtailed}\,(t) = P_{pv,generated}\,(t) - P_{curtail,}(t) \qquad (2)$$

where $P_{pv,curtailed}\,(t)$ is the curtailed PV power at time t, $P_{pv,generated}\,(t)$ is the total PV power generated at time t,and $P_{curtail,}(t)$ is the power curtailed at time t to prevent overgeneration.

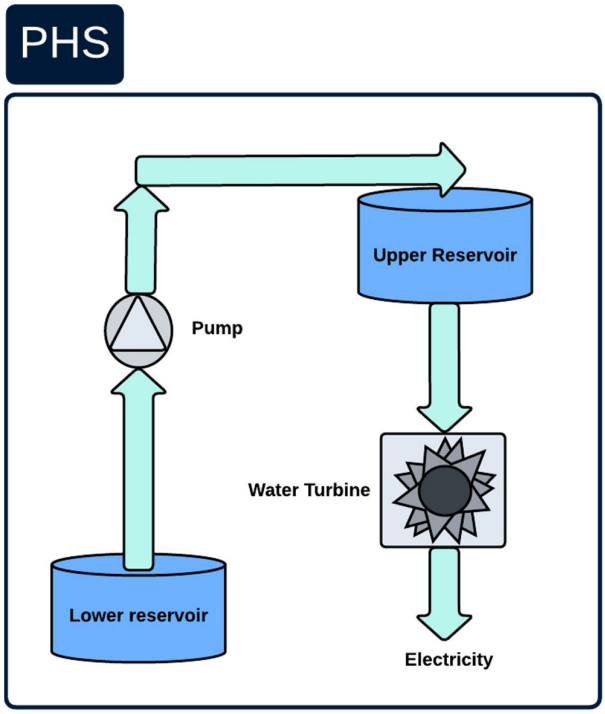

FIGURE 2. Pumped hydro storage system.

2) ESS MODELING

ESSs play a pivotal role in the context of HPPs by serving as reservoirs for surplus energy generated from RESs and bridging energy deficits when needed. In this research, we classify both batteries and PHS as instances of ESS [20]. To elucidate, the energy of an ESS, E(t) can be conceptually simplified with a dynamic model represented as follows:

$$E(t) = E(t-1) - \delta_t P_{ess}(t) \qquad (3)$$

where δ_t is a parameter that influences the change in energy state per unit of power. The $P_{ess}(t)$ is the DC power of the battery, assuming a positive value when the battery injects power into the grid and a negative value when it is in charging mode. The effective control of battery charging and discharging stands as one of the most critical elements for enhancing the overall efficiency of the HPP. On an hourly basis, the battery SoC is expressed as follows:

$$SoC(t) = SoC(t-1).(1-\sigma) + \eta_b.\left(P_{pv}(t) - \frac{1}{\eta_{inv}}P_l(t)\right) \quad (4)$$

where P_l is the load power, σ is the battery's self-discharge rate and η_b is the battery efficiency.

3) DIESEL GENERATOR (DG) MODELING

The utilization of a DG as a backup system is imperative due to the inherent unpredictability of power generation from both PV and BESS [21]. In off-grid energy systems, DGs have the dual purpose of regulating voltage and enhancing reliability [22]. On an hourly basis, the quantity of fuel consumed by the DG (F_{DG}) is a function of the output power (P_{DG}) as follows:

$$F_{DG}(t) = a.(P_{DG}(t))^2 + b.P_{DG}(t) + c \quad (5)$$

where the variables a, b, and c are coefficients or parameters that determine the relationship between the fuel consumption $F_{DG}(t)$ of the DG and its output power $P_{DG}(t)$. Regarding the fuel price FP_{DG}, the models for calculating both hourly and annual fuel costs can be expressed through (6) and (7), respectively.

$$FC_{DG}(t) = FP_{DG}.F_{DG}(t) \quad (6)$$

$$FC_{DG,year}(t) = \sum_{t=1}^{8760} FC_{DG}(t) \quad (7)$$

In terms of environmental impact, CO2 constitutes 99.4% of the leading greenhouse gases emitted from the combustion of diesel fuel, and some other gases such as methane, but in this paper the focus will be on CO2 [23].

4) PHS MODELING

As shown in **FIGURE 2**, PHS is a widely recognized and commercially viable technology for storing electrical energy, consisting of a separated pump/motor unit and a turbine/generator, and accomplished by harnessing the potential energy of water [24]. In this sophisticated storage approach, surplus energy is harnessed during off-peak periods to elevate water from a lower reservoir to a higher one. Subsequently, during peak demand periods, this elevated water is strategically released, permitting it to flow through a hydro turbine, thus converting its stored potential energy into electrical power generation [25].

The power of the pump (P_p) can be expressed by (8):

$$P_p(t) = \frac{\rho g H_p.q_p(t)}{\eta_p} = c_p.q_p(t) \quad (8)$$

where ρ is water density (kg/m^3), H_p (m) is pumping head, g is the gravitational acceleration (m/s^2), $q_p(t)$ is the function of the pump flow rate (m^3/s), η_p is the pump efficiency, and the generating coefficient of the pump (kmW/m^3) is c_p.

The power of the turbine (P_t) can be expressed by (9):

$$P_t(t) = \eta_t \rho g H_{net}.q_t(t) = c_t.q_t(t) \quad (9)$$

where H_{net} (m) is the net head, $q_t(t)$ is the function of the turbine flow rate (m^3/s), η_t is the turbine efficiency and generating coefficient of the turbine (kmW/m^3) is c_t.

The stored potential energy in the upper reservoir is expressed by (10) [26]

$$E_c = \frac{\eta_t.\rho.g.H.V}{3.6 \times 10^6} \quad (10)$$

where E_c is the energy storage capability of the water reservoir (kWh) and V is the volume of the upper reservoir (m^3). The total stored quantity of water in the upper reservoir can be expressed by (11):

$$Q_{UR}(t) = Q_{UR}(t-1)(1-\alpha) + q_p(t) - q_t(t) \quad (11)$$

where $Q_{UR}(t)$ is the total quantity of water and α is the leakage loss. The SoC of the upper reservoir (UR) is represented in terms of the water level within the storage tank, where the water level serves as a proxy for SoC

This relationship is described by the following (12) [27].

$$SoC(t) = \frac{Q_{UR}(t)}{Q_{UR,max}} \quad (12)$$

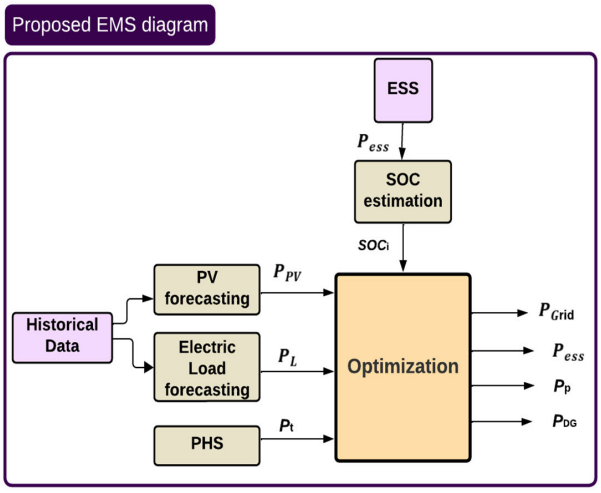

FIGURE 3. Energy management system block diagram.

5) ENERGY MANAGEMENT SYSTEM

FIGURE 3 shows the proposed EMS that provides the power references for the ESS power (P_{ess}), the Pump and turbine power for the PHS (P_t, P_p), the desired grid power (P_G), and the desired DG power (P_{DG}). The EMS inputs are the predicted solar power (P_{pv}), expected load (P_L), turbine power (P_t), and the initial conditions for the battery charge (SoC_i).

The power plant within the microgrid is typically owned and managed by a local entity or consortium. This ownership structure allows for localized control and efficient management of the energy resources, enhancing the reliability and resilience of the power supply. The EMS plays a crucial role in efficiently managing and optimizing the operation of various components in a hybrid energy system [28]. These components include PHS, PV, ESS, the grid, and DG. The Diesel Generator (DG) is connected to the local distribution network in our microgrid setup. This configuration allows the DG to operate as a backup power source within the microgrid, ensuring reliability and stability of the power supply. The DG supports the local energy needs and provides supplementary power during periods of insufficient renewable energy generation or battery storage. EMS regulates the operation of the PHS system by deciding when to release water from the upper reservoir to generate electricity through hydro turbines based on real-time energy needs. During electricity generation, power is produced by the hydro turbine, and this electricity can be utilized within the energy management system (EMS) to meet real-time energy needs. Any excess electricity generated, such as from PV, can be directed by the EMS to various storage systems, including pumping water from the lower reservoir to the upper reservoir in the PHS system when demand is low or electricity is cheap, converting it into potential energy [29].

Also, EMS monitors PV panel output, deciding whether to use, store, or export the generated solar electricity. EMS controls the charging and discharging of ESS, like batteries, to store excess electricity for later use during high-demand or expensive periods. It manages the connection with the grid, deciding when to import or export electricity to optimize performance and minimize costs. In case of power deficits or insufficient RESs, EMS can activate the DG as a backup, determining its start and stop times for system reliability and efficiency [20].

The power balance principle where the power generated must match the power consumed and stored in the ESS, transferred to or from the grid, and managed by the PHS system to maintain a stable and balanced electrical system. The power balance of the proposed HPP can be modeled by equation (13). This equation ensures that the total power in the system is conserved, and any excess generation or deficit is accounted for in terms of these components.

$$\begin{aligned} &P_l\,(t) + P_{DG}(t) - P_{pv}\,(t) \\ &\quad - P_{ess,ch}\,(t) + P_{ess,dis}\,(t) - P_G\,(t) \\ &\quad + P_p\,(t) - P_t\,(t) = 0 \end{aligned} \tag{13}$$

The equation states that the sum of power generated by Diesel Generators (P_{DG}) and the electrical load (P_l) should equal the sum of power generated by PV panels (P_{pv}), power used for ESS (P_{ess}), power imported or exported from or to the grid (P_G), and power generated or consumed by the PHS system (P_{phs}). The EDE controller regulated the charging and discharging of the ESS to ensure that the PV operated at optimum efficacy. If the PV output is greater than the necessary load, the extra power is used to fill the ESS while the ESS is released if the PV output is less than the required load [30].

B. MILP OPTIMIZATION

In MILP, the objective function and constraints are linear, but some decision variables can only take integer values, while others can take continuous values. The MILP method solves the optimization problem by formulating it as a mathematical model and then using specialized algorithms to find the optimal solution [31]. One common approach is to use a branch-and-bound algorithm, which involves recursively partitioning the feasible solution space and solving linear programming problems at each node until the optimal solution is found [21]. This paper will use the MILP to find the optimal solution that represents the lowest cost.

FIGURE 4 shows a detailed flowchart of the EMS algorithm employed in this study to solve a MILP optimization problem for HPP integrating an ESS, DG, PHS, PV, and load. The flowchart represents the decision-making process of the EMS, which includes multiple checks to ensure optimal operation. Each component in the flowchart is distinctly color-coded for clarity, ensuring that the progression of the algorithm is easily understandable. Key steps and decision points are highlighted to emphasize their importance in the EMS process. The feedback correction was used similarly to the paper [32], which will help reduce the scheduling errors resulting from forecasting errors. The objective is to minimize the use of the ESS while meeting the load demand.

The Total Cost Functions for this HPP can be expressed as follows

$$J_{total} = J_{ESS} + J_{PV} + J_{Load} + J_{DG} + J_{grid} + J_{phs} \tag{14}$$

where J_{Load}, J_{PV}, J_{DG},J_{phs} and J_{ESS} are the cost functions of the load, PV, DG, PHS, and ESS, respectively.

$$J_{ESS} = C_{purchased,ess} - C_{sold,ess} \tag{15}$$

where J_{ESS} a function of the cost of ESS is, $C_{purchased,ess}$ is a cost of purchased power, and $C_{sold,ess}$ is a cost of sold power.

$$\begin{aligned} J_{ESS} = &\sum_{t=1}^{t+N} \Delta t.C_{GRID}\,(t) \\ &.\left(\eta_{ch,ESS}.P_{ess,ch}\,(t) - \frac{1}{\eta_{dis,ESS}} P_{ess,dis}\,(t)\right) \end{aligned} \tag{16}$$

where N corresponds to the duration of the forecasted horizon for a specific time (t) given and $(t+N)$ is the cumulative sum. C_{GRID} is the cost of grid power, and it is equal to $C_{purchased}$ when purchasing power from the grid, while C_{GRID} is equal to C_{sold} when selling power to the grid. $\eta_{ch,ESS}$ is the charging efficiency of the ESS while $\eta_{dis,ESS}$ is the discharging efficiency of the ESS. $P_{ch,ESS}\,(t)$ is the ESS charging power while $P_{dis,ESS}\,(t)$ is the ESS discharging power [33].

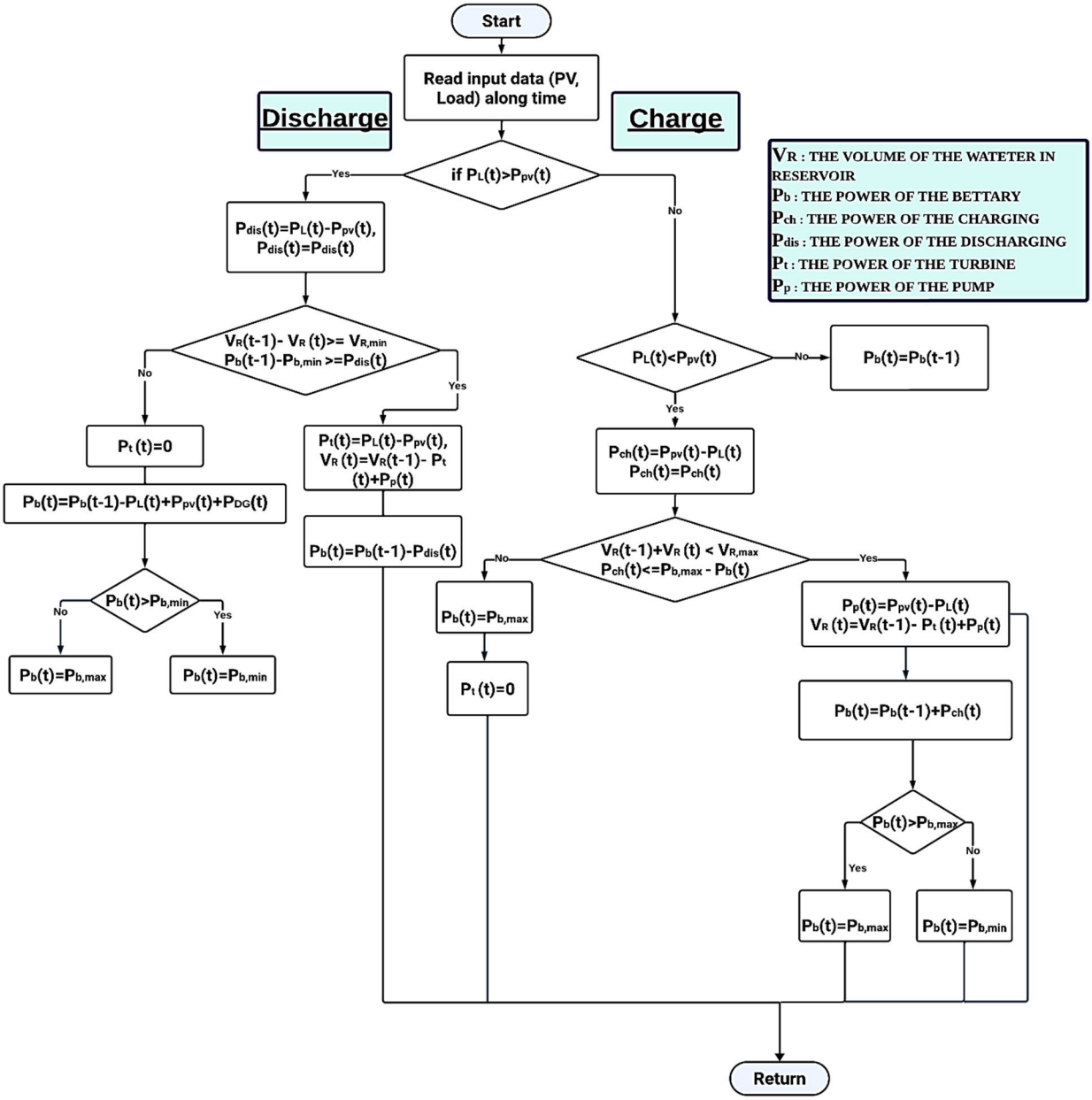

FIGURE 4. Flowchart of the EMS algorithm.

The PV's power values are given, so the function of the cost of PV power is expressed as follows:

$$J_{PV} = \sum_{t=1}^{t+N} \Delta t . P_{pv}(t) . C_{pv} \tag{17}$$

where J_{PV} is a function of the cost of the PV. The C_{pv} is the constant cost of the PV.

$$J_{Load} = \sum_{t=1}^{t+N} \Delta t . C_{GRID}(t) . (P_{purchased}(t) - P_{sold}(t)) \tag{18}$$

$$J_{load} = C_{purchased,l} - C_{sold,l} \tag{19}$$

where J_{Load} is a function of the cost of the Load power, $C_{purchased}$ is a cost of purchased power, and C_{sold} is a cost of sold power.

J_{DG} is represented as the combination of the expenses linked to the fuel necessary for generating sufficient energy to meet load demands and operate the generation facility, along with the emissions-related costs. By knowing the quantities of gas produced when burning diesel fuel, the emission costs can be formulated as a function of fuel consumption, as follows:

$$J_{DG} = \sum_{t=1}^{t+N} \Delta t \cdot \left(\frac{(P_{purchased}(t) - P_{sold}(t)).F}{P_{DG}^{max}} \cdot (C_f + C_m \alpha_{co_2}) \right) \tag{20}$$

where P_{DG}^{max} the DG produces he maximum power, C_f is the cost of fuel per liter, α_{co_2} and C_m are the gas mass associated with burning fuel and the cost of said gases, and F is the amount of diesel used per kWh. The function of the cost of PHS is expressed as follows:

$$J_{phs} = \sum_{t=1}^{t+N} \Delta t . C_{GRID}\,(t)\,. \left(\eta_p . P_p\,(t) - \frac{1}{\eta_t} P_t\,(t)\right) \tag{21}$$

where η_p is the pump efficiency of the PHS while η_t is the turbine efficiency of the PHS. $P_p\,(t)$ is the PHS pumping power while $P_t\,(t)$ is the PHS turbine power. Now the total cost function can be simplified as follows:

$$\begin{aligned} J_{total} &= \sum_{t=1}^{t+N} \Delta t . \Big(P_{pv}\,(t)\,.C_{pv} + C_{GRID}\,(t)\,[\eta_{ch,ESS} . P_{ess,ch}\,(t) \\ &\quad - \frac{1}{\eta_{dis,ESS}} P_{ess,dis}\,(t) + \big(P_{purchased}\,(t) - P_{sold}\,(t)\big) \\ &\quad + \eta_p . P_p\,(t) - \frac{1}{\eta_t} . P_t\,(t)] \\ &\quad + \frac{(P_{purchased}\,(t) - P_{sold}\,(t)) . F . (C_f + C_m . \alpha_{co_2})}{P_{DG}^{max}}\Big) \end{aligned} \tag{22}$$

Since the total cost functions are constrained by a multiple of the constraints that affect the system's behavior as shown below:

s.t (1), Power Balance:

$$\begin{aligned} &P_l\,(t) + P_{DG}(t) - P_{pv}\,(t) \\ &\quad - P_{ess,ch}\,(t) + P_{ess,dis}\,(t) \\ &\quad - P_G\,(t) + P_p\,(t) - P_t\,(t) = 0 \end{aligned} \tag{23}$$

s.t (2), SoC Balance:

$$\begin{aligned} SoC\,(t) &= SoC\,(t-1) \\ &\quad + \frac{1}{Q_{ESS}} \left(\eta_{ch,ESS} . P_{ess,ch}\,(t) - \frac{1}{\eta_{dis}} P_{ess,dis}\,(t)\right) \end{aligned} \tag{24}$$

s.t (3), ESS Control:

$$ESS = \begin{cases} x . P_{ess,ch-min} \le P_{charge}\,(t) \le x . P_{ess,ch-max} \\ y . P_{ess,dis-min} \le P_{dis}\,(t) \le y . P_{ess,dis-max} \\ SoC_{min} \le SoC_{min}\,(t) \le SoC_{max} \\ x, y \in \{0, 1\} \\ y = 1 - x \end{cases} \tag{25}$$

where x & y are integer variables responsible for and representing the state of the behavior of ESS either charging or discharging. Q_{ESS} is the maximum capacity of the ESS (kWh).

s.t (4), State of water Balance:

$$V_R\,(t) = V_R\,(t-1)\,.(1-\delta) + \frac{1}{E_R} \left(\eta_p . P_p\,(t) - \frac{1}{\eta_t} . P_t\,(t)\right) \tag{26}$$

where δ is the evaporation and leakage loss. During pumping and power generation, V_R is the state of water volume in the reservoir of the PHS at time t, which must be maintained between its minimum and maximum values, $V_{R,min}$ and $V_{R,max}$, and is calculated considering the previous volume, evaporation and leakage losses, and the efficiencies and power of the pump and turbine.

s.t (5), PHS Control:

$$PHS = \begin{cases} x . T_{min} \le T\,(t) \le x . T_{max} \\ y . P_{p,min} \le P_p\,(t) \le y . P_{p,max} \\ V_{R,min} \le V_R\,(t) \le V \\ x, y \in \{0, 1\} \\ y = 1 - x \end{cases} \tag{27}$$

where T is the turbine value, and when it is 0% the valve is fully closed. Otherwise, when T is 100% the valve is fully open.

s.t (6), DG Control:

The diesel generator power is bounded between maximum and minimum values as

$$P_{DG} = \big\{P_{DG,min}\,(t) < P_{DG}\,(t) < P_{DG,max}(t) \tag{28}$$

C. STOCHASTIC GRADIENT DESCENT OPTIMIZATION

Stochastic gradient descent (SGD) is an optimization algorithm commonly used in machine learning and deep learning to minimize the loss function of a model by updating the model parameters based on the gradient of the loss function computed on a randomly selected subset of the training data [34]. SGD has many benefits and one of the most important is efficiency with large datasets. In many machine learning tasks, datasets can be massive, and processing the entire dataset in each iteration of the optimization process can be computationally expensive. SGD addresses this issue by using a random subset of the data in each iteration. This significantly speeds up the training process [35]. This random sampling introduces noise in the gradients but allows the algorithm to converge faster to a reasonable solution since it can take steps in the direction of the optimal solution more frequently. In each iteration, the algorithm computes the gradient of the loss function with respect to the parameters for the selected batch. It updates the parameters in the opposite direction of the gradient. The step size is controlled by a learning rate, which determines the magnitude of the update. The process continues for a fixed number of epochs or until the convergence criteria are met. The main advantage of stochastic gradient descent is its computational efficiency, which makes it suitable for large-scale problems. However, it can be sensitive to the learning rate, which may need to be adjusted during training, and it may converge to a suboptimal solution if the initial learning rate is too high or too low. Various extensions of the basic algorithm, such as mini-batch gradient descent and momentum, have been proposed to improve its performance and stability [34].

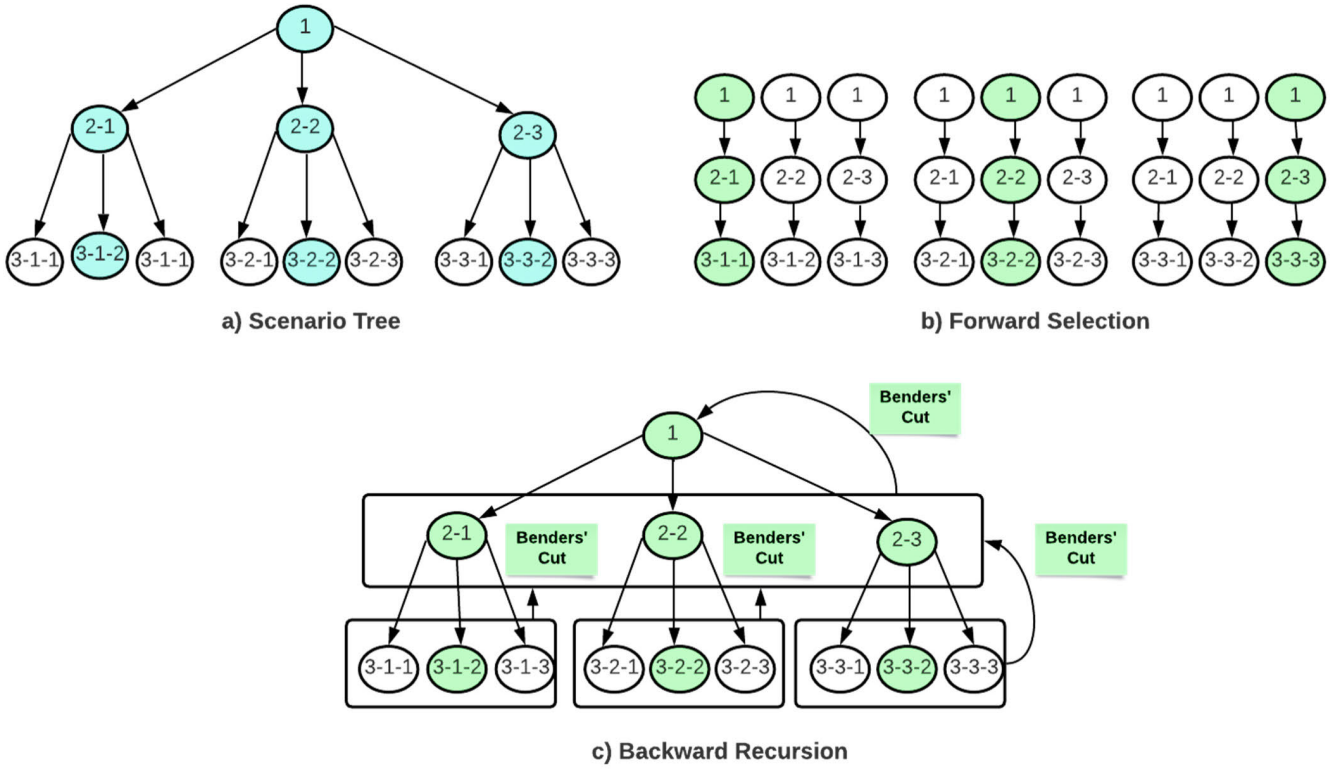

FIGURE 5. SDDP optimization (Scenario Tree).

The objective function and constraints must be defined to finalize the HPP modeling, which includes PV, ESS, and load for SGD optimization. As done previously in MILP optimization, the objective function and constraints will remain the same for both optimization methods.

The objective of the optimization problem is to minimize the total cost of electricity generation and storage over a specified time period.

The cost function of the Energy Storage System (ESS) is designed to capture its behavior concerning the State of Charge (SoC) in a stochastic gradient descent optimization framework. The primary goal is to minimize the total cost associated with electricity generation and storage over a specified timeframe, taking into account both the charging and discharging costs [36]. The stochastic gradient descent algorithm can be used to find the optimal values of the PV power and ESS power that satisfy the constraints and minimize the total cost of electricity generation and storage, subject to the constraints on the PV generation, load demand, and ESS capacity [37], [38].

D. MULTI-STAGE STOCHASTIC OPTIMIZATION PROGRAM

The multistage-stochastic process, whose distribution is known, allows for a comprehensive understanding of the system's behaviour under uncertainty. The process's manifestation may be viewed at distinct times, and remedial actions are conceivable. This yields an iterated observation-decision scheme in which a choice of remedial actions are made after each observation of the stochastic process. This approach is particularly beneficial for several reasons such as energy management to balance the supply and demand of multiple energy resources, including RESs, conventional sources, and energy storage. Also, multi-stage optimization allows for the optimal control of energy storage systems over time, including charging, discharging, and state-of-charge management while allowing for integrated long-term and short-term planning [39]. A discrete-time horizon t was considered and suppose that the set is either finite or infinitely countable. Afterward, we will limit ourselves to limited horizons. The index identified the time points, and it was written as t = {1, 2,..., t} or t = {1, 2,...} [14].

The equations (22) - (28) can be represented as a multi-stage stochastic linear program as the following formula:

$$h_t(x_t, b_t) = \min_{x_t} c_t x_t + \mathbb{E}_{b_{(t+1|b_t)}} h_{t+1}(x_t, b_{t+1}) \quad (29)$$

$$\text{s.t.} \quad A_t x_t = B_t x_{t-1} + b_t : \pi_1 \quad (30)$$

$$x_t \geq 0 \quad (31)$$

where t = 2,...,T, x_t is the decision variables at a certain stage, π_t is the dual variables associated with the constraints, and the expression $(\mathbb{E}_{b_{(t+1|b_t)}} h_{t+1}(x_t, b_{t+1}))$ denotes the estimated cost function for stage t+1, based on decisions (x_t), which is the vector of decision variables at time t, made in stage t, where bt+1 represents the realization of the random

parameter for that case, while b_t is a vector representing external inputs or disturbances at time t. A_t, B_t are matrices defining the relationship between current and previous state variables.

Also, the general T-stage stochastic linear program is shown below in (32) - (34):

$$\min_{x_t} c_t x_t + \mathbb{E}_{(b_2 \mid b_1)} h_2 (x_t, b_2) \tag{32}$$

$$\text{s.t.} \quad A_1 x_1 = B_1 x_0 + b_1 : \pi_1 \tag{33}$$

$$x_t \geq 0 \tag{34}$$

The decision variables at a certain stage, represented by vector x_t, including electricity purchases from the grid, the charge and discharge power of the ESS, and the battery's state of charge (SoC). The target functions for minimizing the total cost, considering present and future stage costs, are described in (29) and (32). The structural constraints of the model, (30) and (33), the specific scenario involves power balance and charge balance (22) and (23). The dual variables (πt) obtained from the structural constraints are utilized to create a piece-wise linear estimation of the future cost function through Benders' decomposition technique. Equations (31) and (34) define the state transitions in the optimization model. A_t, B_t are matrices that relate the state and decision variables across different time periods, while b_t represents external inputs or disturbances. The dual variables π_t are associated with these constraints, providing necessary conditions for optimality. Equations (31) and (34) impose straightforward restrictions on the decision variables, such as (26) and (27). In the objective function presented in equation (32), The expression $c_t x_t + \mathbb{E}_{(b_2 \mid b_1)} h_2 (x_t, b_2)$ denotes the estimated cost function for stage 2, considering decisions (x_1) made in stage 1. In this context, b_2 represents a random parameter that influences the system's condition at stage 2. Likewise, in equation (29), $\mathbb{E}_{b_{(t+1 \mid b_t)}} h_{t+1} (x_t, b_{t+1})$ calculates the projected cost function for stage t+1, based on decisions (x_t) made in stage t, where b_{t+1} represents the realization of the random parameter for that case [40]. To date, the most advanced approach for solving multi-stage stochastic linear programming is the SDDP method. SDDP addresses the computational complexity of Dynamic

Programming (DP) by approximating the future cost function with piece-wise linear functions known as Benders' cuts, which are progressively included. This iterative process continues until a specific stopping measure is satisfied [41]. **FIGURE 5** provides a visual representation of how SDDP works for a three-stage problem, although it's important to note that the actual tree sizes can be large[43].

In the SDDP procedure, once a sampled scenario tree is provided, the forward pass begins by sampling the pathways in the tree. Throughout the problem-solving process, these paths are taken into account. In the forward pass, models represented by (32) - (34) are solved at each time stage using the simplex approach. Benders' cuts obtained from previous iterations for the corresponding stage are incorporated as additional constraints to enhance the approximation of future costs and improve decision-making. The average cost of all the sampled forward pathways serves as an estimation of the anticipated future cost. At the final stage, the entire predicted cost is calculated, serving as the upper bound for the problem. Solving the first stage problem provides a lower bound for the sampled problem. The upper and lower bounds converge after a finite number of iterations, and the process can be terminated based on a convergence criterion. During the convergence process, if the upper and lower bound costs fail to achieve the desired level of convergence, an additional iteration of SDDP is executed. New forward pathways are sampled individually in each cycle. The algorithm then conducts the backward pass to achieve the desired convergence level. During the backward pass, additional Benders' cuts are computed at specific stages to reflect the projected future cost function better. Cuts are not used at the final stage since there are no future costs [13]. The marked nodes in **FIGURE *5 (c)*** indicate the selected nodes in the backward pass for each iteration. Benders' cut for stage t is computed using equations (35)-(37).

$$\theta_t + G_t x_t \geq g_t \tag{35}$$

$$G_t = \sum \omega_{t+1 \in \Delta(\omega_t)} \pi_{t+1}^{\omega_{t+1}} B_{t+1} \tag{36}$$

$$g_t = \sum \omega_{t+1 \in \Delta(\omega_t)} h_{t+1}^{\omega_{t+1}} - G_t [x_t^{\omega_t}]^k \tag{37}$$

where the future cost obtained from the forward pass is represented by θt, the dual variables are denoted by $\pi_{t+1}^{\omega_{t+1}}$, and the optimal cost is indicated by $h_{t+1}^{\omega_{t+1}}$ from the solved linear problem for stage (t+1) [40].

The backward pass is unable to solve all of the sampled forward pathways that were solved in the forward path. The SDDP can calculate the Benders' cuts by selecting a subset of sampled forward pathways. Because the backward pass estimation takes longer than the forward pass estimation, the number of paths chosen can be lowered to accelerate convergence. Following the completion of the backward pass for every stage, a separate set of forward pathways is sampled from the scenario tree to represent the cumulative cuts gained from the backward pass of every iteration for every stage of the system [43].

III. SIMULATION AND RESULTS

A MATLAB code has been used for the simulation, the "**Optimproblem"** function is used to define an optimization problem with decision variables for the power generated by the HPP, the power charging/discharging of the ESS, and the energy capacity of the ESS over time. The case studies provided in this manuscript illustrate a larger scale than typical microgrid setups. This approach is intended to demonstrate the scalability and flexibility of the proposed energy dispatch management system. While the examples exceed the conventional microgrid scale, they highlight the system's potential for larger applications and integration of various energy resources. Additionally, the system is equally applicable to smaller, more conventional microgrid setups, offering broad versatility in energy management. The objective function is

to minimize the total power generated by the HPP over the simulation period. The economic model considered in this study includes the capital costs of the PV system, batteries, and other components, as well as the operational costs related to energy dispatch and grid interactions. The operation and maintenance (O&M) costs of the Energy Storage System (ESS) were excluded from this analysis for several reasons:

- Focus on Capital and Operational Optimization: Our study primarily aims to optimize the capital and operational expenditures associated with energy dispatch and system efficiency, which are critical to our research objectives.
- Comparative Analysis Objective: This research is designed to compare different energy dispatch strategies under various tariff schemes, where the inclusion of relatively constant O&M costs would not significantly impact the comparative results.
- Simplified Economic Model: To simplify the model and concentrate on the main variables affecting optimization, we excluded O&M costs. Future research will incorporate these costs for a more comprehensive economic assessment.

Constraints are included to ensure power balance, energy storage capacity limits, and the relationship between power charging/discharging of the ESS and energy storage over time. The pricing mechanism for the microgrid is based on Time-of-Use (ToU) tariffs, which reflect the varying cost of electricity during different times of the day. This approach incentivizes users to shift their energy consumption to periods when electricity is cheaper, thereby improving cost-effectiveness and load management within the microgrid. The Real-time hourly electricity prices of Chicago are used to calculate the cost and used for the tariff cost as well as presented in **TABLE 2** [41].

TABLE 2. Time-of-use (TOU) tariff.

Time of Use		Tariff ($/kWh)
(12 AM to 6 AM)	Off Peak	0.0195
(6 AM to 6 PM)	Partial-Peak	0.04
(6 PM to 12 AM)	Peak	0.031

A. MILP

The cost data used in the analysis consisted of real-time electricity pool prices, sampled at 15-minute intervals, which determined the cost of purchasing or selling electricity. Forecasted data for both PV generation and load demand were provided. The figures presented in the analysis depict the system's performance over 24 hours. **FIGURE 6 (a)** and **FIGURE 6 (b)** display the PV generation and load demand profiles for the entire day. **FIGURE 6 (d)** presents the grid power profile for a system empty of (PHS), whereas **FIGURE 7 (a)** showcases the grid power profile for a system integrated with PHS over a day. These plots representations delineate the changes in grid power within predefined upper and lower bounds, which are influenced by the status of the

TABLE 3. System parameters.

Parameter	*Value*
SOC-init	50%
battEnergy	100 MWh
$\eta_{charge,ESS}$	0.90
$\eta_{discharge,ESS}$	0.85
Q-ESS	100 MWh
Δt	15 min
$P_{charge,ESS-max}$	20 MW
$P_{discharge,ESS-min}$	-20 MW
$\text{PV}_{Purchasing}$ Cost	1500 $/kW
η_p	75 %
η_t	80 %
$\forall_{intial}$	40 %
α_{co_2}	2.557 kg/L
C_m	0.05 $/kg
C_f	1.5 $/L
F	0.08 L/kW
P_{DG}^{max}	20 MW
P_{DG}^{min}	10 kW
E_R	9.2 MWh
$\forall_{min}$	15%
$\forall_{max}$	80%

(ESS). When the ESS is discharging, the grid power exhibits a positive value, signifying the draw of electricity from the grid to fulfil demand. When the load is relatively miniature, the ESS with PHS is capable of handling the load while also generating power for it. However, if the load were to double, the grid would commence power generation to support the ESS and PHS in meeting the increased load demand. Notably, as evidenced in **FIGURE 6 (b)** and **FIGURE 7 (a)**, the cumulative net grid power for the system without PHS is lesser than that for the system incorporating PHS, amounting to 521 MW and 678 MW, respectively. **FIGURE 6 (c)** and **FIGURE 7 (c)** show the power profile of the ESS without and with PHS integration, respectively. **FIGURE 6 (c)** the minimum ESS power registers at (−17 MW), slightly higher than the corresponding value depicted in **FIGURE 7 (c)** (−15 MW), while the standard minimum ESS power stands at (−20 MW).

This discrepancy arises from the interplay between the grid, DG, and the charging/discharging cycles of the ESS, all while adhering to specified constraints and anticipated power demands. The operational capacity of the ESS is defined by its battery capacity. By minimizing ESS operations while considering SoC the plot underscores charging and discharging patterns. The initial SoC of the system, depicted in **FIGURE 6 (e)** without PHS, is 50%. It commences discharging for the first 6 hours of the day, followed by a charging phase until it reaches 53%. Subsequently, another discharge phase ensues, succeeded by a charging phase ultimately restoring the SoC to 50% in response to peak load hours. Conversely, for a system incorporating PHS, **FIGURE 7 (e)** illustrates a similar SoC pattern within the PHS system. Here,

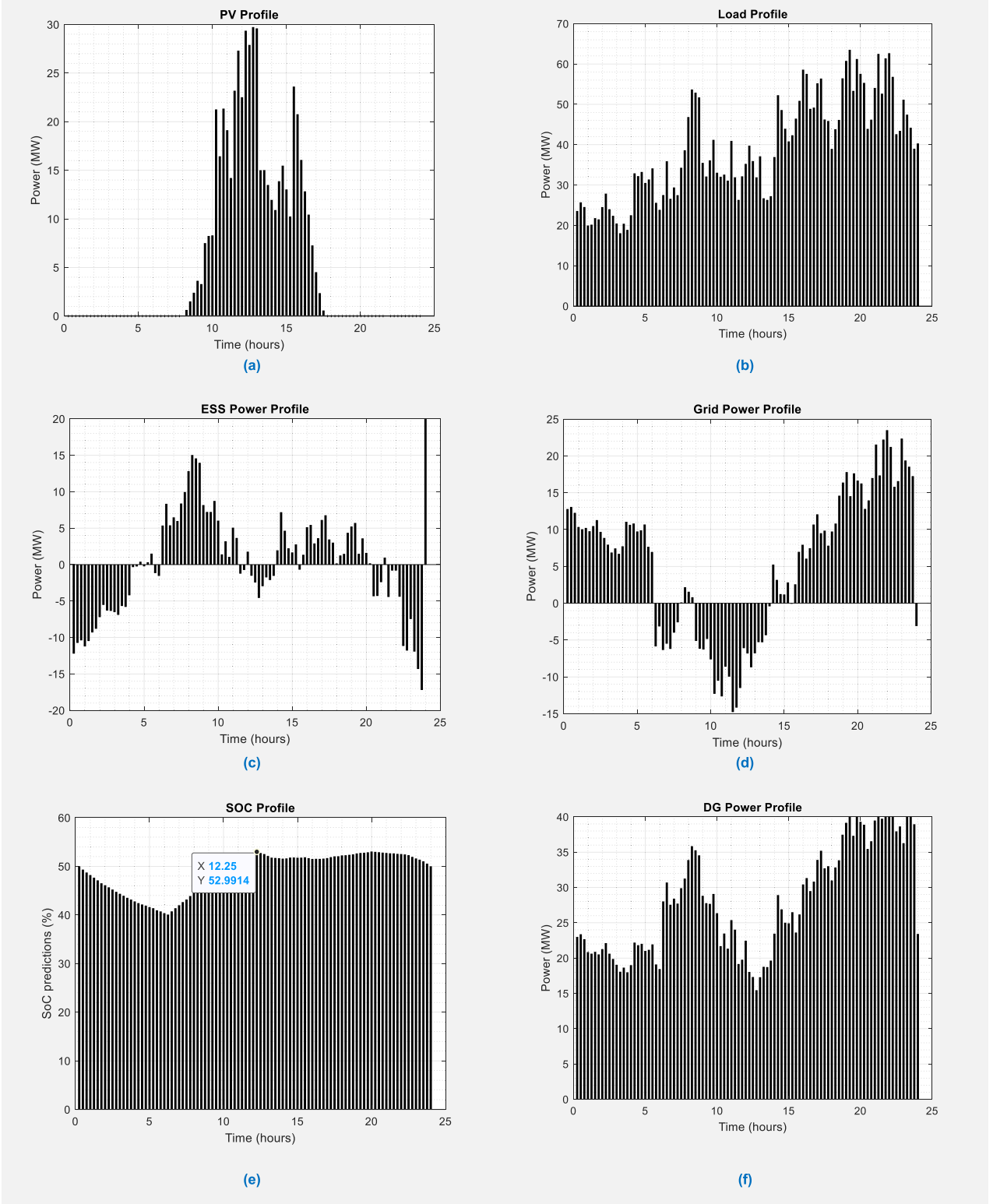

FIGURE 6. Results of the MILP optimization for a Hybrid Energy System (HES) combining PV, DG, and ESS. (a) the system's PV profiles, (b) the system's Load profiles, (c) ESS power profile (PV, DG, ESS), (d) grid profile (PV, DG, ESS), (e) SoC profiles (PV, DG, ESS), and (f) DG profile (PV, DG, ESS).

the SOC initiates charging after the initial 6 hours of the day and continues,until it reaches 52%. It has to be noted that the SoC decreases/increases with the discharging/charging of the battery with the negative/positive sign of the power,

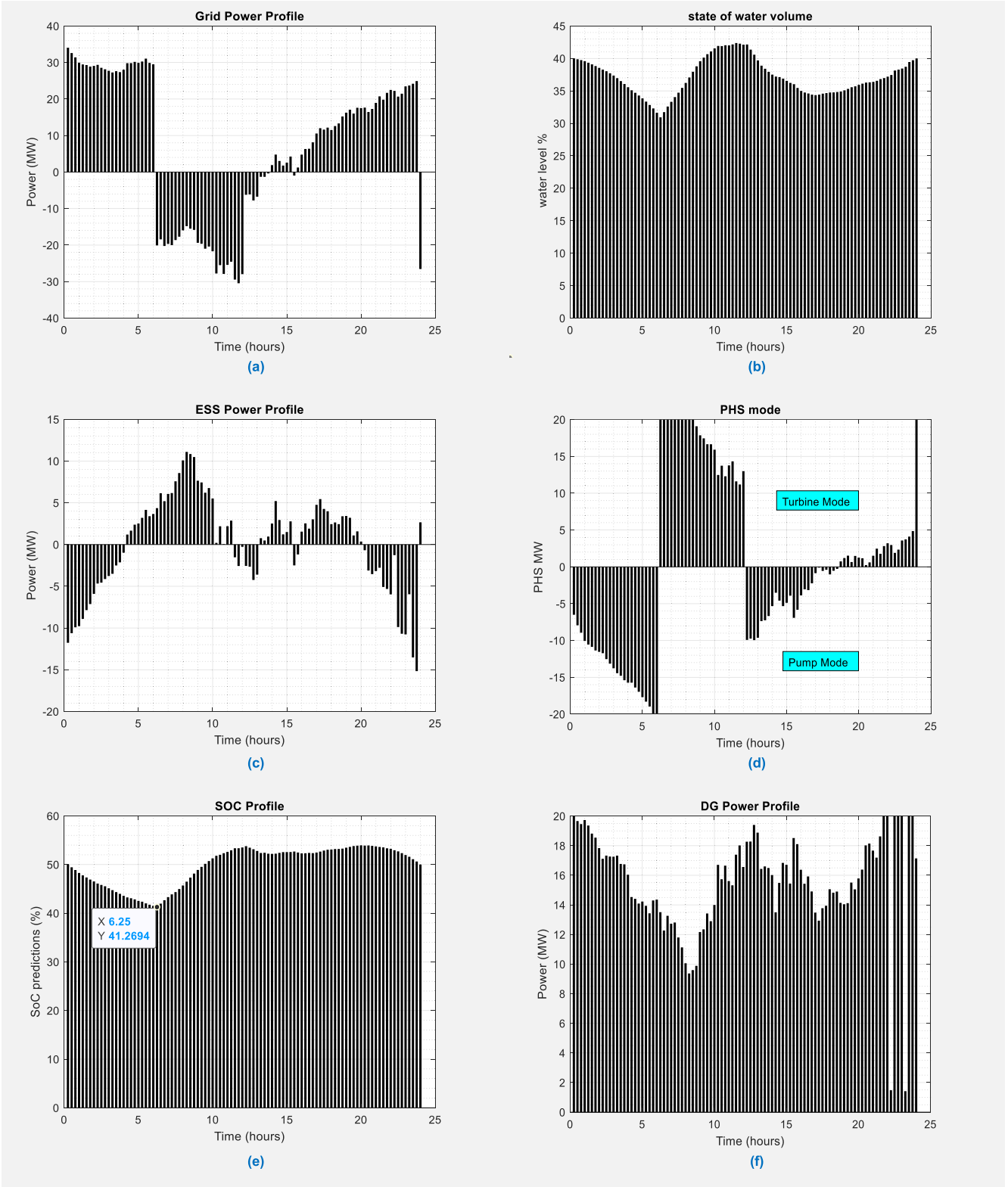

FIGURE 7. Results of the MILP optimization for a Hybrid Energy System (HES) combining PV, DG, PHS, and ESS. (a) grid profile (PV, DG, ESS, PHS), (b) water level state profile (PV, DG, ESS, PHS), (c) ESS power profile (PV, DG, ESS, PHS), (d) PHS profile (PV, DG, ESS, PHS), (e) SoC profiles (PV, DG, ESS, PHS), and (f) DG profile (PV, DG, ESS, PHS).

respectively. In the system comprising DG, PV, ESS, and PHS, **FIGURE 7(b)** illuminates the water level state within the PHS system. Initially set at 40% of its capacity, the water level volume decreases until it reaches 21% during the first

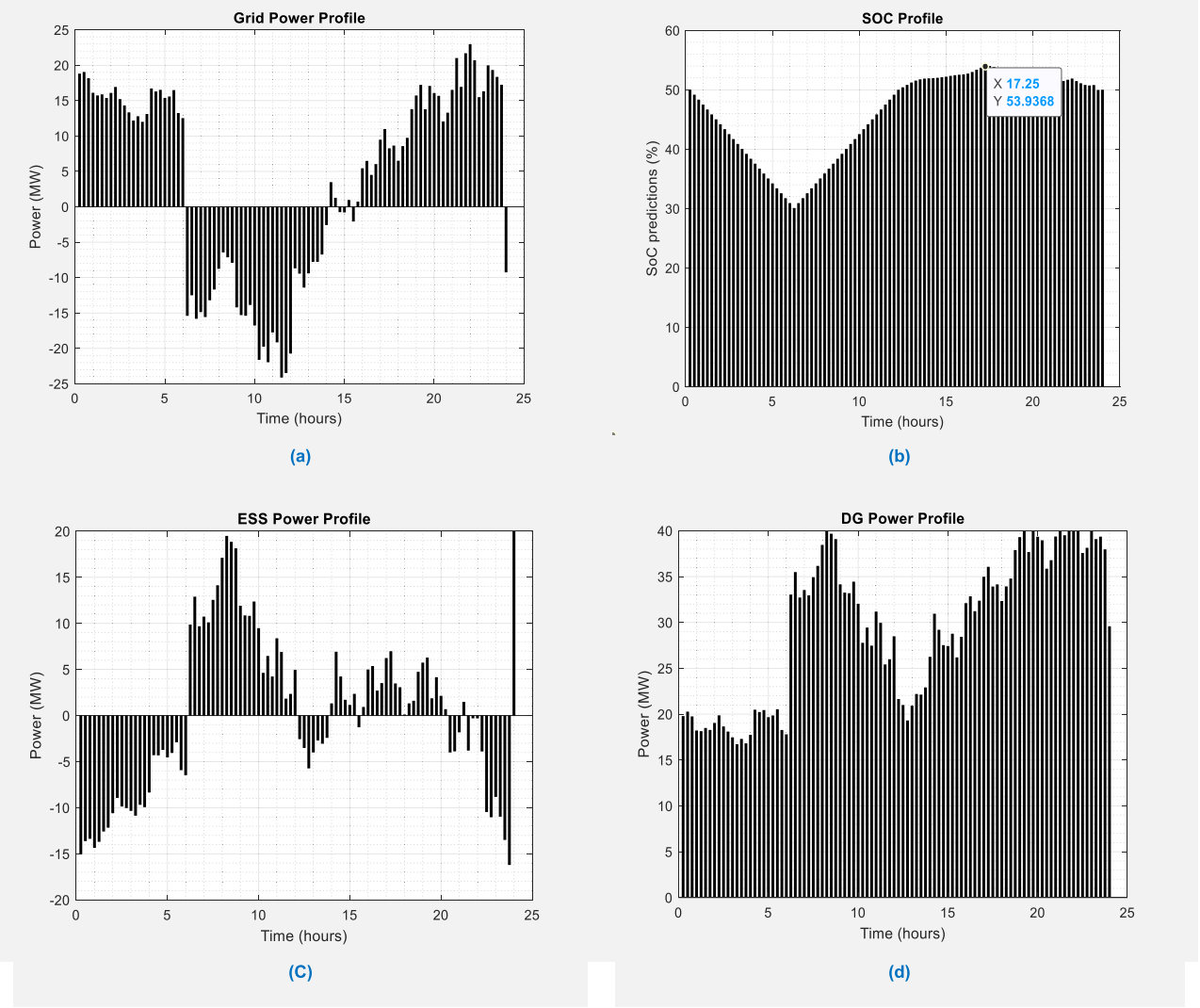

FIGURE 8. Results of the SDDP optimization for a Hybrid Energy System (HES) combining PV, DG, and ESS. (a) ESS power profile (PV, DG, ESS), (b) grid profile (PV, DG, ESS), (c) SoC profiles (PV, DG, ESS), and (d) DG profile (PV, DG, ESS).

6 hours of the day, followed by an ascent phase until it reaches 44.1%. This decrement denotes a period of heightened electrical demand surpassing the ESS's capacity alone to satisfy the load, prompting the PHS system to generate supplementary electricity. While both PHS and ESS serve as energy storage systems, they operate distinctively. PHS stores energy as potential energy by pumping water to an upper reservoir and subsequently releasing it through turbines to generate electricity as needed. During instances of elevated demand exceeding supply, such as peak periods or low PV generation, both PHS and ESS discharge stored energy to the grid, aiding in grid stabilization and mitigating the necessity for DG. Moreover, **FIGURE 7 (d)** and **FIGURE 9 (d)** elucidate the PHS mode for both MILP and SDDP methods, respectively. When operating as a pump, the PHS system consumes electrical energy to transfer water from a lower reservoir to an upper reservoir, effectively storing energy. This pump mode entails the PHS system acting as a load and consuming power, yielding a negative power output. Conversely, when functioning as a generator or turbine, the system releases stored water from the upper reservoir to the lower reservoir, converting potential energy into electrical energy. In this generator mode, the PHS system acts as a generator, producing electrical power and yielding a positive power output. The inclusion of PHS in the HES augments its energy storage capabilities and enhances grid stability while mitigating dependence on DG and grid power. Strategic coordination and optimization of PHS and ESS alongside other system components can yield improved performance, cost efficiency, and environmental sustainability.

B. SDDP

The SDDP method is employed to optimize the operation of ESS while considering uncertainty, which is represented by 5 stages, each stage has 10 different scenarios. These scenarios are generated based on stochastic variations in load

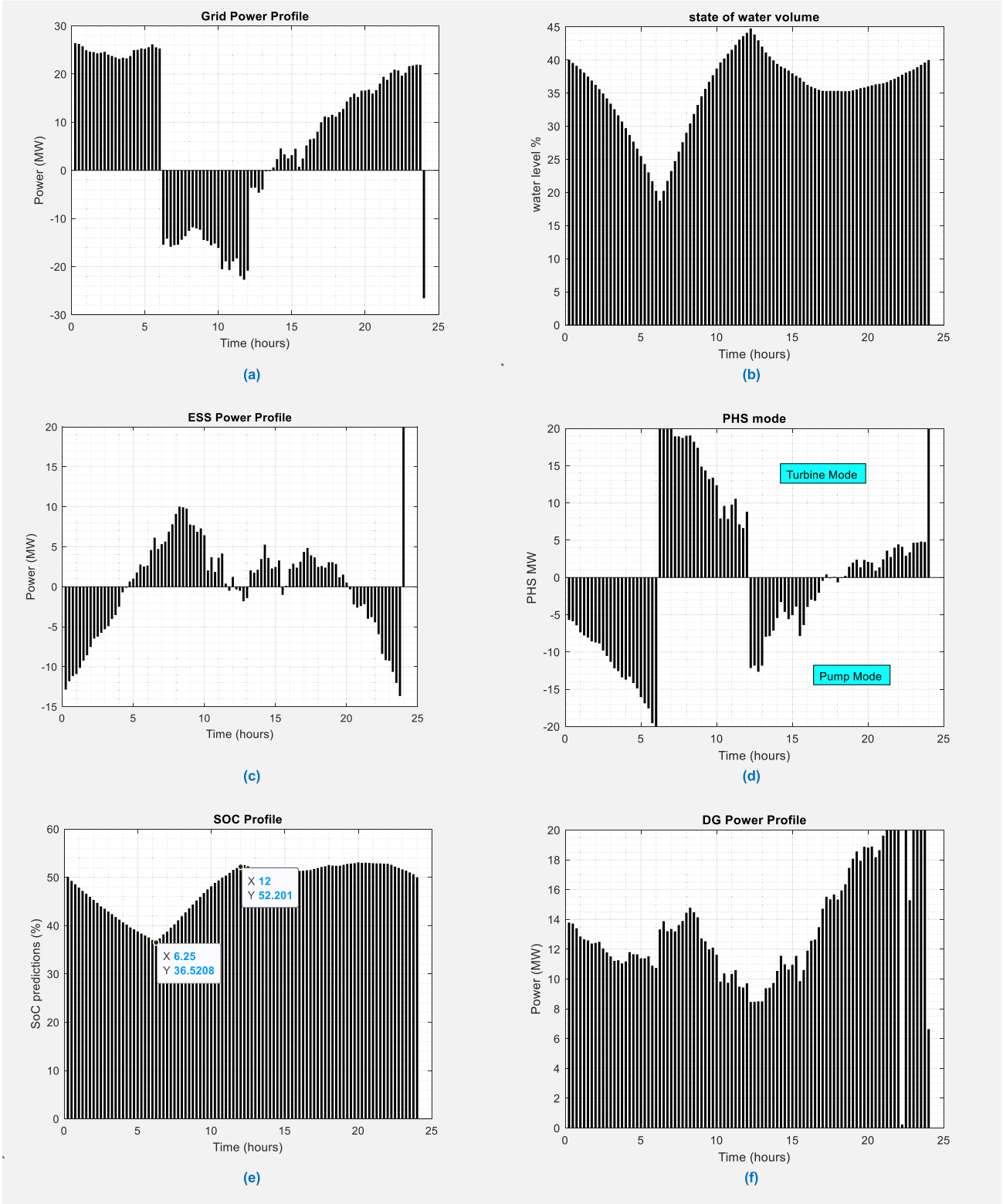

FIGURE 9. Results of the SDDP optimization for a Hybrid Energy System (HES) combining PV, DG, PHS, and ESS. (a) grid profile (PV, DG, ESS, PHS), (b) water level state profile (PV, DG, ESS, PHS), (c) ESS power profile (PV, DG, ESS, PHS), (d) PHS profile (PV, DG, ESS, PHS), (e) SoC profiles (PV, DG, ESS, PHS), and (f) DG profile (PV, DG, ESS, PHS).

and PV generation profiles. To generate sample scenarios for uncertain parameters at each stage, changes in load may arise from variations in these uncertain factors across different scenarios or stages. These sample scenarios serve as distinct

possible realizations of uncertain variables, such as PV generation or load demand, encountered within the optimization problem. These scenarios are instrumental in estimating the expected value of the objective function associated with the constraints. Including scenarios in the optimization process enhances the robustness of decision-making for ESS operation. By considering various scenarios, the algorithm can make informed decisions that lead to reduced energy purchases and more efficient utilization of the ESS. This approach enables better management of the ESS's SoC while minimizing operational costs. **FIGURE 8 (a)** presents the grid power profile for a system empty of PHS, whereas **FIGURE 9(a)** showcases the grid power profile for a system integrated with PHS over a day. Notably, as evidenced in **FIGURE 8 (a)** and **FIGURE 9 (a)**, the cumulative net grid power for the system without PHS is lesser than that for the system incorporating PHS, amounting to 370 MW and 678 MW, respectively. **FIGURE 8 (c)** and **FIGURE 9 (c)** show the power profile of the ESS without and with PHS integration, respectively. These plots indicate periods of charging and discharging while adhering to all provided constraints and anticipated power requirements. The ESS's operational capacity is constrained by its battery capacity. Positive ESS power values contribute to an increase in SoC, while negative ESS power values result in a decrease in SoC. **FIGURE 8 (b)** presents the SoC percentage profile throughout the day for the system without PHS. The plot highlights charging and discharging patterns, indicating that the initial SOC of the system is 50%. It begins discharging for the first 6 hours of the day, followed by a charging phase until it reaches 53.9%. Subsequently, it initiates another discharge phase, ultimately returning to 50% SOC in response to peak load hours. However, for a system that also includes PHS, **FIGURE 9 (e)** illustrates a similar SOC pattern. Here, the SOC begins discharging for the first 6 hours of the day and continues until it reaches 52.2%. Constraints on the minimum and maximum SoC of the ESS are rigorously enforced for each scenario, ensuring that the ESS operates within predefined and safe boundaries. Through optimization across scenarios, the algorithm strives to strike a balance between maximizing ESS utilization and maintaining SoC within acceptable limits. Upon analyzing **FIGURE 8 (d)** and **FIGURE 6 (f)**, show the changes in DG power within the system without PHS. These figures depict minimal changes in DG values, with the maximum DG power peaking at 40 MW. This nominal variance can be ascribed to the persistent and considerable load demand, which maintains a consistently high level. Furthermore, the absence of PHS exacerbates the situation by limiting the system's flexibility in adjusting power outputs to meet fluctuating demands. Conversely, upon review of **FIGURE 7 (f)** and **FIGURE 9 (f)**, illustrating the changes in DG power within the system integrated with PHS, with large dynamic changes. These visual representations portray dynamic shifts in DG values, indicative of a system that incorporates both PHS and Energy Storage Systems (ESS). This integration facilitates more agile and adaptable energy management strategies, resulting in a scenario where the maximum DG power is capped at 20 MW. Such responsiveness is made possible by the complementary nature of PHS and ESS, allowing for efficient balancing of supply and demand dynamics within the system. For a system comprising DG, PV, ESS, and PHS, **FIGURE 9 (b)** visualizes the water level status within the PHS system. Initially, the water level is set at 40% of its total capacity. As indicated at $t = 1$, the water level decreases to 19%, and then it increases to 45%. This decline reflects a period of heightened electrical demand that surpassed the ESS's capacity to independently meet the load. Consequently, during this period, the PHS system commences electricity generation to complement the power supply. Both PHS and ESS are categorized as energy storage systems, although they operate differently. One commonality between PHS, ESS, and the grid is their capacity to store surplus energy when generation exceeds demand and release stored energy when demand exceeds generation. This capability contributes to grid stability, facilitates load balancing, and allows for the storage of excess energy for future utilization. Constraints are integrated into the code to ensure that the SoC remains within predefined limits. In the context of the SDDP algorithm, the results obtained from solving the optimization problem for each scenario provide valuable insights into the optimal operation of the HPP. These insights encompass the intricate relationship between the grid, SoC, and the ESS, as well as strategies for minimizing ESS operation while accounting for SoC considerations. By thoroughly analyzing the outcomes generated by the SDDP algorithm, you can gain a deeper understanding of the optimal control decisions governing grid, ESS, PHS, and PV power under various scenarios.

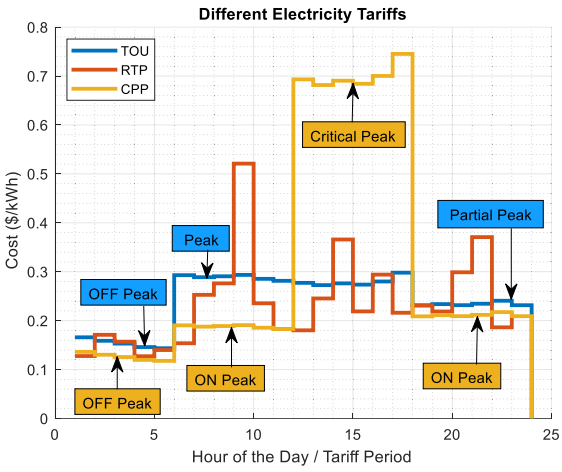

FIGURE 10. Different electricity tariffs.

C. TOTAL ELECTRICITY COST OF DIFFERENT TARIFFS & CO2 EMISSION COST

In this research, the Real Time Pricing (RTP) scheme refers to a scenario where electricity rates are directly tied to the ever-changing electricity market prices. These rates are not

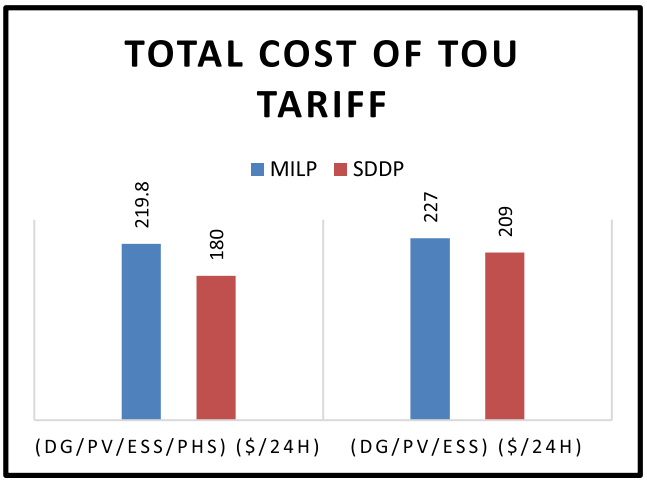

FIGURE 11. The convergence analysis and final optimal cost comparison.

fixed in advance and typically fluctuate hourly. TOU tariffs, conversely, represent the most used approach to pricing that varies with time. Under TOU, each day is divided into two to five intervals, each having a set electricity rate. This division and rate determination process occur monthly. In the Critical Peak Pricing (CPP) scheme, either TOU or RTP rates generally apply for most days throughout the year. However, a few specific days within the year witness rate adjustments during certain hours that coincide with peak electricity demand provides an overview of the various tariff structures considered in the Chicago case study [41]. **TABLE 4** presents the CO2 emission costs for both MILP and SDDP, revealing that the CO2 cost is lower in the case of SDDP. Interestingly, the system without PHS exhibits higher CO2 costs compared to the system with PHS. The values presented in **TABLE 4** were calculated using the following equations:

$$CO_{2,emission} = \sum_{t=1}^{t+N} E_{DG}(t) + E_{grid}(t) \tag{38}$$

$$CO_{2,cost} = CO_{2,emission}.C_{CO_2} \tag{39}$$

where the $E_{DG}(t)$ is the carbon emissions from the diesel generator at time t, $E_{grid}(t)$ is the carbon emissions from grid power usage at time t, and C_{CO_2} is the cost per Kg of CO2 emissions. These equations represent the methodology used to derive the CO2 cost and CO2 emissions for the hybrid power plant system. **TABLE 5** and **TABLE 6** provide a comparison of the total optimized and base electricity costs between the MILP and SDDP methods. These tables reflect the overall energy costs of the proposed HES, contrasting the optimized and base costs for the following pricing schemes: RTP, TOU, and CPP. **TABLE 5** displays the total cost for the MILP method, indicating that the system without PHS incurs higher costs (e.g., 227 $/24h) than the system with PHS (e.g., 219.8 $/24h). On the other hand, **TABLE 6** reveals the total cost for the SDDP method, where the system without PHS (e.g., 209 $/24h) exhibits

TABLE 4. Daily CO^2 emission cost.

Optimization Method	MILP Method (DG/PV/ ESS/PHS)	MILP Method (DG/PV/ESS)	SDDP Methode (DG/PV/ ESS/PHS)	SDDP Methode (DG/PV/ESS)
CO^2 Cost ($/24h)	10.2	11	8.3	9.51
CO^2emission (kg/24h)	200	215	160	185

TABLE 5. Daily operational Cost for MILP.

Total cost of different Tariff	TOU	RTP	CPP
(DG/PV/ESS/PHS) ($/24h)	219.8	205	225.2
(DG/PV/ESS) ($/24h)	227	215	235

TABLE 6. Daily operational Cost for SDDP.

Total cost of different Tariff	TOU	RTP	CPP
(DG/PV/ESS/PHS) ($/24h)	180	175	193
(DG/PV/ESS) ($/24h)	209	198.1	216.4

higher costs than the system with PHS (e.g., 180 $/24h). It's noteworthy that the SDDP approach consistently results in lower total costs than MILP. The rationale behind the SDDP method's cost-effectiveness, particularly in complex systems dealing with uncertainty and multiple scenarios, lies in its ability to consider a broad spectrum of scenarios and their associated probabilities. This approach offers a more accurate representation of real-world uncertainties in energy systems. In contrast, MILP primarily relies on deterministic models, rendering it more conservative and less adaptable to variable conditions. Furthermore, SDDP employs probabilistic models to represent uncertainties more faithfully, whereas MILP often relies on deterministic approximations that can lead to suboptimal decisions and higher costs. The convergence analysis and optimal cost comparison clearly indicate that the proposed SDDP method outperforms the MILP method in optimizing the energy dispatch for hybrid power plants. The SDDP algorithm not only converges more efficiently but also achieves lower overall costs, validating its effectiveness in real-time energy management scenarios as shown in **FIGURE 11** illustrates the PV and load profiles after introducing white noise. The added white noise, characterized by a standard deviation of the noise is half of the standard deviation of the original signals, introduces stochastic elements into the PV and load data. This randomness serves to simulate real-world unpredictability and variability in energy generation and consumption patterns. The effects of this noise on the outcomes of Stochastic Dual Dynamic Programming (SDDP) and Mixed-Integer Linear

Programming (MILP) optimization methods are explored in the subsequent analysis. Introducing white noise to the data can enhance the robustness of the SDDP approach, making it more adaptable and resilient to variations. SDDP is explicitly designed to manage uncertainty, and the introduction of noise effectively simulates real-world unpredictability. Consequently, the SDDP method is likely to yield more reliable and robust solutions, as evident in **TABLE 8**, where the total cost without white noise is slightly higher than the total cost with white noise. Conversely, incorporating white noise into MILP can significantly elevate the complexity of the optimization problem. MILP models may encounter challenges when handling noisy data, resulting in more intricate and time-consuming computations. Additionally, MILP may struggle to identify the most cost-effective solutions in the presence of noisy data, possibly leading to suboptimal outcomes. This, in turn, can result in higher total electricity costs, as evident in **TABLE 7**, where the total cost without white noise is lower than the total cost with white noise.

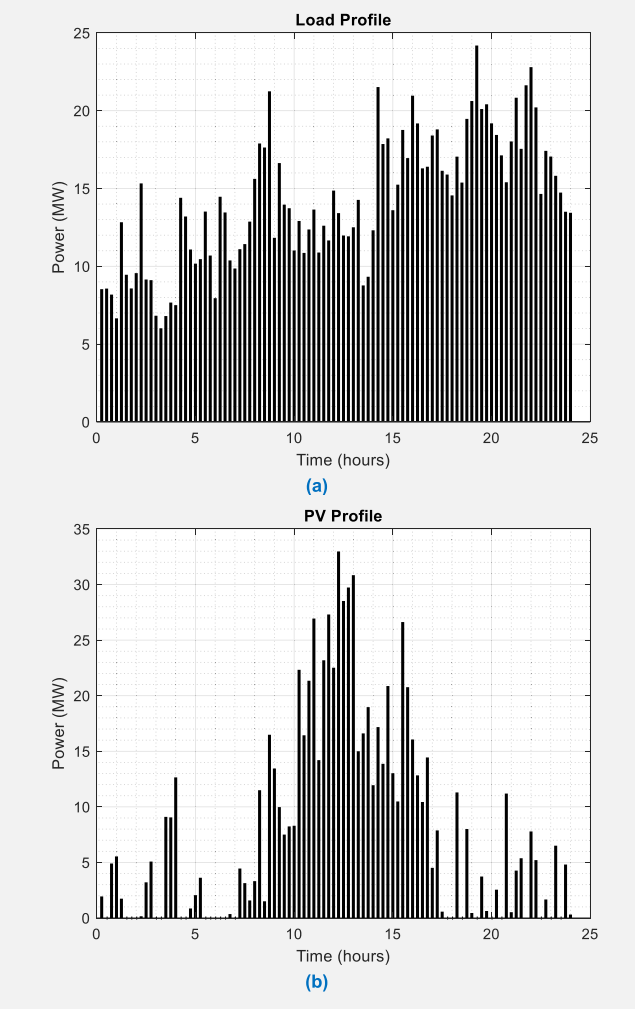

FIGURE 12. The effect of white noise that being added with a standard deviation that is half (0.5) of the original signals of PV and Load. (a) Load profile, (b) PV profile.

TABLE 7. The daily operational Cost for MILP with showing the presence of uncertainty in the load and PV profiles, with the standard deviation specified as 0.5 MW.

Total cost of different Tariff	TOU	RTP	CPP
(DG/PV/ESS/PHS) ($/24h)	221.3	209	227.5
(DG/PV/ESS) ($/24h)	229.4	216	241

TABLE 8. The daily operational Cost for SDDP with showing the presence of uncertainty in the load and PV profiles, with the standard deviation specified as 0.5 MW.

Total cost of different Tariff	TOU	RTP	CPP
(DG/PV/ESS/PHS) ($/24h)	181	173	195
(DG/PV/ESS) ($/24h)	210.2	199.1	216

IV. CONCLUSION

In conclusion, in this research, complex challenges of optimizing HPPs were tackled by integrating various RESs and storage systems. The focus was on a hybrid setup combining PV systems, BESS, DG, and PHS to enhance energy management and minimize operational costs and carbon emissions. An advanced EDE was developed using MILP) and SDDP. The SDDP algorithm demonstrated superior performance in optimizing the discharge and charge profiles of the BESS, resulting in lower total costs and reduced carbon emissions compared to the MILP method. The SDDP approach consistently achieved lower total costs than the MILP approach. The total cost for the system with PHS using SDDP was 180 $/24h, significantly lower than the MILP cost of 219.8 $/24h. Findings indicated that the SDDP method also reduced CO2 emissions, with the SDDP approach emitting 160 kg of CO2 per day compared to 200 kg with the MILP method. Introducing stochastic elements, such as white noise into PV and load data, demonstrated the robustness of the SDDP method in handling real-world unpredictability, further validating its effectiveness for dynamic energy management. This study highlights the importance of advanced optimization techniques in managing hybrid power plants. The proposed SDDP algorithm not only improves cost efficiency but also enhances environmental sustainability by reducing emissions. The flexibility and scalability of this approach make it suitable for various applications, from small microgrids to larger power systems. These findings contribute significantly to the ongoing efforts to optimize renewable energy integration, reduce costs, and promote sustainable energy solutions in the evolving energy landscape. The scalability of the proposed system is one of its key strengths. Although the case studies presented in this paper are on a larger scale, the energy dispatch management system is designed to be adaptable to both large and small setups. This flexibility makes it suitable for a wide range of applications, from localized microgrids to more

extensive power systems. Future work may include further analysis and case studies focusing on smaller, conventional microgrid setups to illustrate the system's broad applicability.

ACKNOWLEDGMENT

The statements made herein are solely the responsibility of the authors.

REFERENCES

[1] M. Azeroual, T. Lamhamdi, H. El Moussaoui, and H. El Markhi, "Simulation tools for a smart grid and energy management for microgrid with wind power using multi-agent system," *Wind Eng.*, vol. 44, no. 6, pp. 661–672, Dec. 2020, doi: 10.1177/0309524x19862755.

[2] H. A. U. Muqeet and A. Ahmad, "Optimal scheduling for campus prosumer microgrid considering price based demand response," *IEEE Access*, vol. 8, pp. 71378–71394, 2020, doi: 10.1109/ACCESS.2020.2987915.

[3] M. Al-Saadi, M. Al-Greer, and M. Short, "Reinforcement learning-based intelligent control strategies for optimal power management in advanced power distribution systems: A survey," *Energies*, vol. 16, no. 4, p. 1608, Feb. 2023, doi: 10.3390/en16041608.

[4] V. Khare, S. Nema, and P. Baredar, "Solar–wind hybrid renewable energy system: A review," *Renew. Sustain. Energy Rev.*, vol. 58, pp. 23–33, May 2016, doi: 10.1016/j.rser.2015.12.223.

[5] L. Moretti, M. Astolfi, C. Vergara, E. Macchi, J. I. Pérez-Arriaga, and G. Manzolini, "A design and dispatch optimization algorithm based on mixed integer linear programming for rural electrification," *Appl. Energy*, vols. 233–234, pp. 1104–1121, Jan. 2019, doi: 10.1016/j.apenergy.2018.09.194.

[6] M. Liu, F. L. Quilumba, and W.-J. Lee, "Dispatch scheduling for a wind farm with hybrid energy storage based on wind and LMP forecasting," *IEEE Trans. Ind. Appl.*, vol. 51, no. 3, pp. 1970–1977, May 2015, doi: 10.1109/TIA.2014.2372043.

[7] P. Roy, J. He, and Y. Liao, "Cost minimization of battery-supercapacitor hybrid energy storage for hourly dispatching wind-solar hybrid power system," *IEEE Access*, vol. 8, pp. 210099–210115, 2020, doi: 10.1109/ACCESS.2020.3037149.

[8] N. Lou, Y. Zhang, Y. Wang, Q. Liu, H. Li, Y. Sun, and Z. Guo, "Two-stage congestion management considering virtual power plant with cascade hydro-photovoltaic-pumped storage hybrid generation," *IEEE Access*, vol. 8, pp. 186335–186347, 2020, doi: 10.1109/ACCESS.2020.3030637.

[9] B. Wang, G. Cai, and D. Yang, "Dispatching of a wind farm incorporated with dual-battery energy storage system using model predictive control," *IEEE Access*, vol. 8, pp. 144442–144452, 2020, doi: 10.1109/ACCESS.2020.3014214.

[10] H. Rezk, M. Al-Dhaifallah, Y. B. Hassan, and H. A. Ziedan, "Optimization and energy management of hybrid photovoltaic-diesel-battery system to pump and desalinate water at isolated regions," *IEEE Access*, vol. 8, pp. 102512–102529, 2020, doi: 10.1109/ACCESS.2020.2998720.

[11] A. J. Lamadrid, D. L. Shawhan, C. E. Murillo-Sánchez, R. D. Zimmerman, Y. Zhu, D. J. Tylavsky, A. G. Kindle, and Z. Dar, "Stochastically optimized, carbon-reducing dispatch of storage, generation, and loads," *IEEE Trans. Power Syst.*, vol. 30, no. 2, pp. 1064–1075, Mar. 2015, doi: 10.1109/TPWRS.2014.2388214.

[12] F. Hafiz, M. A. Awal, A. R. D. Queiroz, and I. Husain, "Real-time stochastic optimization of energy storage management using deep learning-based forecasts for residential PV applications," *IEEE Trans. Ind. Appl.*, vol. 56, no. 3, pp. 2216–2226, May 2020, doi: 10.1109/TIA.2020.2968534.

[13] M. Gr, J. Schweiger, F. Mathematik, T. Universit, and B. Berlin. (2010). *Application of Multistage Stochastic Programming in Strategic Telecommunication Network Planning*. [Online]. Available: https://www.google.com/%5Cnpapers2://publication/uuid/74BDDFC8-E6DA-4F42-B7E8-F68F0E77EA2C

[14] B. Tan and H. Chen, "Stochastic multi-objective optimized dispatch of combined cooling, heating, and power microgrids based on hybrid evolutionary optimization algorithm," *IEEE Access*, vol. 7, pp. 176218–176232, 2019, doi: 10.1109/ACCESS.2019.2955515.

[15] M. Tostado-Véliz, S. Mouassa, and F. Jurado, "A MILP framework for electricity tariff-choosing decision process in smart homes considering 'Happy Hours' tariffs," *Int. J. Electr. Power Energy Syst.*, vol. 131, Oct. 2021, Art. no. 107139, doi: 10.1016/j.ijepes.2021.107139.

[16] F. Fodhil, A. Hamidat, and O. Nadjemi, "Potential, optimization and sensitivity analysis of photovoltaic-diesel-battery hybrid energy system for rural electrification in Algeria," *Energy*, vol. 169, pp. 613–624, Feb. 2019, doi: 10.1016/j.energy.2018.12.049.

[17] R. Palma-Behnke, C. Benavides, F. Lanas, B. Severino, L. Reyes, J. Llanos, and D. Sáez, "A microgrid energy management system based on the rolling horizon strategy," *IEEE Trans. Smart Grid*, vol. 4, no. 2, pp. 996–1006, Jun. 2013, doi: 10.1109/TSG.2012.2231440.

[18] Z. Belboul, B. Toual, A. Kouzou, L. Mokrani, A. Bensalem, R. Kennel, and M. Abdelrahem, "Multiobjective optimization of a hybrid PV/wind/battery/diesel generator system integrated in microgrid: A case study in Djelfa, Algeria," *Energies*, vol. 15, no. 10, p. 3579, May 2022, doi: 10.3390/en15103579.

[19] O. Skarstein and K. Uhlen, "Design considerations with respect to long-term diesel saving in wind/diesel plants," *Wind Eng.*, vol. 13, no. 2, pp. 72–87, 1989. [Online]. Available: http://www.jstor.org/stable/43749369

[20] Y. Azoumah, D. Yamegueu, P. Ginies, Y. Coulibaly, and P. Girard, "Sustainable electricity generation for rural and peri-urban populations of sub-Saharan Africa: The 'flexy-energy' concept," *Energy Policy*, vol. 39, no. 1, pp. 131–141, Jan. 2011, doi: 10.1016/j.enpol.2010.09.021.

[21] G. He, S. Kar, J. Mohammadi, P. Moutis, and J. F. Whitacre, "Power system dispatch with marginal degradation cost of battery storage," *IEEE Trans. Power Syst.*, vol. 36, no. 4, pp. 3552–3562, Jul. 2021, doi: 10.1109/TPWRS.2020.3048401.

[22] G. El-Jamal, M. Ghandour, H. Ibrahim, and A. Assi, "Technical feasibility study of solar-pumped hydro storage in Lebanon," in *Proc. Int. Conf. Renew. Energies Developing Countries*, Nov. 2014, pp. 23–28, doi: 10.1109/REDEC.2014.7038525.

[23] A.-M. Georgescu, C.-I. Cosoiu, S. Perju, S.-C. Georgescu, L. Hasegan, and A. Anton, "Estimation of the efficiency for variable speed pumps in EPANET compared with experimental data," *Proc. Eng.*, vol. 89, pp. 1404–1411, Jan. 2014, doi: 10.1016/j.proeng.2014.11.466.

[24] F. A. Canales and A. Beluco, "Modeling pumped hydro storage with the micropower optimization model (HOMER)," *J. Renew. Sustain. Energy*, vol. 6, no. 4, Jul. 2014, Art. no. 043131, doi: 10.1063/1.4893077.

[25] T. Ma, H. Yang, L. Lu, and J. Peng, "Pumped storage-based standalone photovoltaic power generation system: Modeling and techno-economic optimization," *Appl. Energy*, vol. 137, pp. 649–659, Jan. 2015, doi: 10.1016/j.apenergy.2014.06.005.

[26] S. Govindasamy, S. R. Balapattabi, B. Kaliappan, and V. Badrinarayanan, "Energy management in microgrids using IoT considering uncertainties of renewable energy sources and electric demands: GBDT-JS approach," *Electr. Eng.*, vol. 105, no. 6, pp. 4409–4426, Aug. 2023, doi: 10.1007/s00202-023-01947-8.

[27] M. Tostado-Véliz, A. A. Ghadimi, M. R. Miveh, D. Sánchez-Lozano, A. Escamez, and F. Jurado, "A novel stochastic mixed-integer-linear-logical programming model for optimal coordination of hybrid storage systems in isolated microgrids considering demand response," *Batteries*, vol. 8, no. 11, p. 198, Oct. 2022, doi: 10.3390/batteries8110198.

[28] B. Bhandari, K.-T. Lee, G.-Y. Lee, Y.-M. Cho, and S.-H. Ahn, "Optimization of hybrid renewable energy power systems: A review," *Int. J. Precis. Eng. Manuf.-Green Technol.*, vol. 2, no. 1, pp. 99–112, Jan. 2015, doi: 10.1007/s40684-015-0013-z.

[29] J. P. Vielma, "Mixed integer linear programming formulation techniques," *SIAM Rev.*, vol. 57, no. 1, pp. 3–57, Jan. 2015, doi: 10.1137/130915303.

[30] C. A. Floudas and X. Lin, "Mixed integer linear programming in process scheduling: Modeling, algorithms, and applications," *Ann. Oper. Res.*, vol. 139, no. 1, pp. 131–162, Oct. 2005, doi: 10.1007/s10479-005-3446-x.

[31] L. Kanaan, L. S. Ismail, S. Gowid, N. Meskin, and A. M. Massoud, "Optimal energy dispatch engine for PV-DG-ESS hybrid power plants considering battery degradation and carbon emissions," *IEEE Access*, vol. 11, pp. 58506–58515, 2023, doi: 10.1109/ACCESS.2023.3281562.

[32] N. Ketkar, "Stochastic gradient descent," in *Deep Learning With Python*. Berkeley, CA, USA: Apress, 2017, pp. 113–132, doi: 10.1007/978-1-4842-2766-4_8.

[33] M. Li, T. Zhang, Y. Chen, and A. J. Smola, "Efficient mini-batch training for stochastic optimization," in *Proc. 20th ACM SIGKDD Int. Conf. Knowl. Discovery Data Mining*, Aug. 2014, pp. 661–670, doi: 10.1145/2623330.2623612.

[34] S. Rajamand, M. Shafie-khah, and J. P. S. Catalão, "Energy storage systems implementation and photovoltaic output prediction for cost minimization of a microgrid," *Electric Power Syst. Res.*, vol. 202, Jan. 2022, Art. no. 107596, doi: 10.1016/j.epsr.2021.107596.

[35] M. A. Hannan, S. B. Wali, P. J. Ker, M. S. A. Rahman, M. Mansor, V. K. Ramachandaramurthy, K. M. Muttaqi, T. M. I. Mahlia, and Z. Y. Dong, "Battery energy-storage system: A review of technologies, optimization objectives, constraints, approaches, and outstanding issues," *J. Energy Storage*, vol. 42, Oct. 2021, Art. no. 103023, doi: 10.1016/j.est.2021.103023.
[36] R. Basmadjian and H. De Meer, "A heuristics-based policy to reduce the curtailment of solar-power generation empowered by energy-storage systems," *Electronics*, vol. 7, no. 12, p. 349, Nov. 2018, doi: 10.3390/electronics7120349.
[37] A. R. de Queiroz and D. P. Morton, "Sharing cuts under aggregated forecasts when decomposing multi-stage stochastic programs," *Oper. Res. Lett.*, vol. 41, no. 3, pp. 311–316, May 2013, doi: 10.1016/j.orl.2013.03.003.
[38] F. Hafiz, A. Rodrigo de Queiroz, P. Fajri, and I. Husain, "Energy management and optimal storage sizing for a shared community: A multi-stage stochastic programming approach," *Appl. Energy*, vol. 236, pp. 42–54, Feb. 2019, doi: 10.1016/j.apenergy.2018.11.080.
[39] V. Guigues, A. Shapiro, and Y. Cheng, "Risk-averse stochastic optimal control: An efficiently computable statistical upper bound," *Oper. Res. Lett.*, vol. 51, no. 4, pp. 393–400, Jul. 2023, doi: 10.1016/j.orl.2023.05.002.
[40] M. V. F. Pereira and L. M. V. G. Pinto, "Multi-stage stochastic optimization applied to energy planning," *Math. Program.*, vol. 52, nos. 1–3, pp. 359–375, May 1991, doi: 10.1007/bf01582895.
[41] *Real Time Hourly Electricity Prices of Chicago*. [Online]. Available: https://hourlypricing.comed.com/live-prices/?date=20231003

FATMA AHMED (Graduate Student Member, IEEE) received the B.Sc. degree (Hons.) in electrical engineering from Qatar University, Qatar, in 2022. She is currently a Research Assistant with the Electrical Engineering Department, Qatar University. Her research interests include machine learning, power electronics, renewable energy, and smart grids.

RASHID AL-ABRI (Senior Member, IEEE) received the B.Sc. degree in electrical engineering from Sultan Qaboos University, Oman, in 2002, the M.Sc. degree in electrical engineering from the Curtin University of Technology, WA, Australia, in 2004, and the Ph.D. degree from the Department of Electrical and Computer Engineering, University of Waterloo, Waterloo, ON, Canada, in 2012. He is currently an Assistant Professor with the Department of Electronics and Communication Engineering (ECE), Sultan Qaboos University. His research interests include power electronics applications, renewable energy, power quality, power systems, smart grid applications, and power system stability.

HASSAN YOUSEF received the B.Sc. (Hons.) and M.Sc. degrees in electrical engineering from Alexandria University, Alexandria, Egypt, in 1979 and 1983, respectively, and the Ph.D. degree in electrical and computer engineering from the University of Pittsburgh, PA, USA, in 1989. He spent 15 years at Alexandria University as an Assistant Professor, an Associate Professor, and a Professor. He joined Qatar University for six years as an Assistant Professor and then an Associate Professor. At Qatar University, he held the position of the Acting Head of the Department of Electrical and Computer Engineering. He was a Visiting Associate Professor with the University of Florida, Gainesville, in Summer 1995. He is currently with the Department of Electrical and Computer Engineering, Sultan Qaboos University, Muscat, Oman. He has supervised 28 M.Sc. theses (completed) and eight Ph.D. dissertations (completed). His publication records include more than 100 papers in refereed journals and international conferences in the area of control systems, nonlinear control, adaptive fuzzy control, and intelligent control applications to power systems and electric drives. He has authored the book *Power System Load Frequency Control: Classical and Adaptive Fuzzy Approaches* (CRC Press, 2017).

AHMED M. MASSOUD (Senior Member, IEEE) received the B.Sc. (Hons.) and M.Sc. degrees in electrical engineering from Alexandria University, Egypt, in 1997 and 2000, respectively, and the Ph.D. degree in electrical engineering from Heriot–Watt University, Edinburgh, U.K., in 2004. He is currently the Associate Dean for Research and Graduate Studies with the College of Engineering, Qatar University, Qatar, and a Professor with the Department of Electrical Engineering, College of Engineering, Qatar University. He has supervised several M.Sc. and Ph.D. students at Qatar University. He has published more than 130 journal articles in the fields of power electronics, energy conversion, and power quality. He holds 12 U.S. patents. His research interests include power electronics, energy conversion, renewable energy, and power quality. He has been awarded several research grants addressing research areas, such as energy storage systems, renewable energy sources, HVDC systems, electric vehicles, pulsed power applications, and power electronics for aerospace applications.